Japanese Journal of Applied Physics
Vol. 44, No. 1B, 2005, pp. 523–529

Intrinsic Electronic Transport through Alkanedithiol Self-Assembled Monolayer

Takhee LEE*, Wenyong WANG† and Mark A. REED‡

Departments of Electrical Engineering, Applied Physics, and Physics, Yale University, P.O. Box 208284, New Haven, CT 06520, U.S.A.

(Received June 21, 2004; revised August 14, 2004; accepted September 9, 2004; published January 24, 2005)

Electronic transport through an alkanedithiol self-assembled monolayer (SAM) is investigated using a nanometer scale device. Temperature-independent current-voltage characteristics are observed, indicating tunneling is the main conduction mechanism. The measured current-voltage characteristics are analyzed with a metal-insulator-metal tunneling model. The inelastic electron tunneling spectroscopy (IETS) study on the octanedithiol device clearly shows the vibrational signatures of molecules. The pronounced IETS peaks correspond to vibrational modes perpendicular to the junction interface, which include the stretching modes of Au-S (at 33 mV) and C-C (at 133 mV), and wagging mode of CH_2 (at 158 mV). Intrinsic linewidths are determined as 1.69 (upper limit), 3.73 ± 0.98, and 13.5 ± 2.4 meV for Au-S, C-C streching modes, and CH_2 wagging mode, respectively. The observed peak intensities and peak widths are in good agreement with theoretical predictions. [DOI: 10.1143/JJAP.44.523]

KEYWORDS: organic devices, self-assembled monolayer, alkanethiol, tunneling, molecular electronics

1. Introduction

In the past several years tremendous progress has been made in the electronic transport characterization of self-assembled monolayers (SAMs).[1,2] Alkanethiol (CH_3-$(CH_2)_{n-1}SH$) is one of the molecular systems that has been studied extensively due to its ability to form a robust SAM on gold surfaces.[3] Recently tunneling has been identified as the main conduction mechanism for alkanemonothiol SAMs formed in a nanometer scale junction,[4] as expected since the Fermi levels of contacts lie within a large HOMO-LUMO gap (HOMO: highest occupied molecular orbital, LUMO: lowest unoccupied molecular orbital) of a short length molecule.[5] In this study, electronic transport through an alkanedithiol SAM (octanedithiol) is investigated (alkanedithiol has thiol groups at both end sides of molecule while alkanemonothiol has a thiol group only on one end). Conduction mechanisms for alkanedithiol are studied by temperature-variable current-voltage ($I(V,T)$) characterization. The transport parameters such as current density, barrier height, and decay coefficient for alkanedithiol are compared with those for alkanemonothiol. The transport for alkanedithiol is further studied by a technique of inelastic electron tunneling spectroscopy (IETS). IETS was developed in the 1960's to study the vibrational spectrum of organic molecules buried inside metal-oxide-metal junctions,[6–8] and has since become a powerful spectroscopic tool for molecular identification and the investigation of chemical bonding.[9] The observed IETS peak intensities and peak widths are compared with theoretical predictions. The purpose of this study is to demonstrate that the IETS technique can be utilized for the unique identification of specific molecular species contained in nanometer scale devices with self-assembled monolayers.

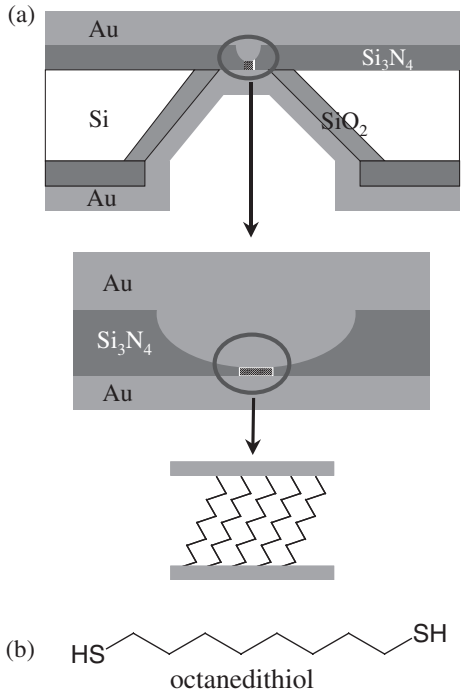

Fig. 1. Schematics of a nanometer scale device used in this study. (a) Top schematic is the cross section of a silicon wafer with a nanometer scale pore etched through a suspended silicon nitride membrane. Middle and bottom schematics show a Au/SAM/Au junction formed in the pore area. (b) Chemical structure of C8-dithiol.

2. Experiment

Electronic transport measurements on an octanedithiol SAM were performed using a nanoscale device (Fig. 1(a))[4] in which a small number of molecules (~ several thousands) are sandwiched between two metallic contacts. This technique provides a stable device structure and makes temperature-variable measurements possible. Details on the device fabrication process have been reported elsewhere.[4,10] In this study, 150 nm gold is thermally evaporated onto the topside of the sample to fill the pore and form one of the metallic contacts. The device is then transferred into a ~5 mM octanedithiol ($HS(CH_2)_8SH$, denoted as C8-dithiol,

*Present address: Department of Materials Science and Engineering, Gwangju Institute of Science and Technology, 1 Oryong-dong, Buk-gu, Gwangju 500-712, Korea. E-mail address: tlee@gist.ac.kr
†Present address: Semiconductor Electronics Division, National Institute of Standards and Technology Gaithersburg, MD 20899, USA. E-mail address: wwang@nist.gov
‡E-mail address: mark.reed@yale.edu

Fig. 1(b)) molecular solution for SAM deposition. The dithiol solution is prepared by adding ~10 μL octanedithiol to 10 mL ethanol. SAM formation is done for 24 h inside a nitrogen filled glove box with an oxygen level of less than 5 ppm. Then the device is rinsed and transferred to an evaporator, where 200 nm Au is deposited on the opposing side to confine the SAM and form an enclosed device. During the second thermal evaporation step (pressure $\sim 10^{-8}$ Torr) liquid nitrogen is flowed through the sample holder to reduce thermal damage to the molecular layer.[4] The device is subsequently packaged and loaded into a cryostat for electrical characterizations between 300 and 4.2 K.

IETS spectra are obtained via a lock-in second harmonic measurement technique.[6,11] A synthesized function generator (Stanford Research Systems DS 345) is used to provide both the AC modulation and the lock-in reference signal. The second harmonic signal (proportional to d^2I/dV^2) is directly measured using a lock-in amplifier (Stanford Research Systems 830), which has also been checked to be consistent with a numerical derivative of the first harmonic signal. Various modulation amplitudes and frequencies are utilized to obtain the spectra. The AC modulation is added to a DC bias (generated by a Yokogawa 7651 DC source) using operational amplifier based custom circuitry.[12]

3. Results

3.1 Tunneling characterization

Tunneling characteristics show a temperature-independent transport behavior, as observed in metal-insulator-metal (M-I-M) systems.[13] Temperature-variable current-voltage ($I(V,T)$) measurement is an important characterization method to unambiguously prove conduction mechanisms (to differentiate tunneling from others, such as thermionic and defect-mediated processes)[4,13] Figure 2(a) is the $I(V,T)$ result for the C8-dithiol device obtained from 300 to 4.2 K. An Arrhenius plot in Fig. 2(b) exhibits little temperature dependence, confirming that tunneling is the main transport mechanism for the C8-dithiol SAM. This result is in good agreement with the tunneling transport characteristics observed previously for alkanemonothiol SAMs.[4]

Figure 3 shows fittings of measured $I(V)$ data with the widely used Simmons tunneling model, eq. (1).[15] The Simmons model expressed the tunneling current density through a barrier in the tunneling regime of $V < \Phi_B/e$ as[14,15]

$$J = \left(\frac{e}{4\pi^2\hbar d^2}\right)\left\{\left(\Phi_B - \frac{eV}{2}\right) \times \exp\left[-\frac{2(2m)^{1/2}}{\hbar}\alpha\left(\Phi_B - \frac{eV}{2}\right)^{1/2} d\right] - \left(\Phi_B + \frac{eV}{2}\right)\exp\left[-\frac{2(2m)^{1/2}}{\hbar}\alpha\left(\Phi_B + \frac{eV}{2}\right)^{1/2} d\right]\right\} \quad (1)$$

where m is the electron mass, h ($= 2\pi\hbar$) is Planck's constant, d is the barrier width, Φ_B is the barrier height, and V is the applied bias. For molecular M-I-M tunneling systems, the Simmons model has been modified with a parameter α[4,14]

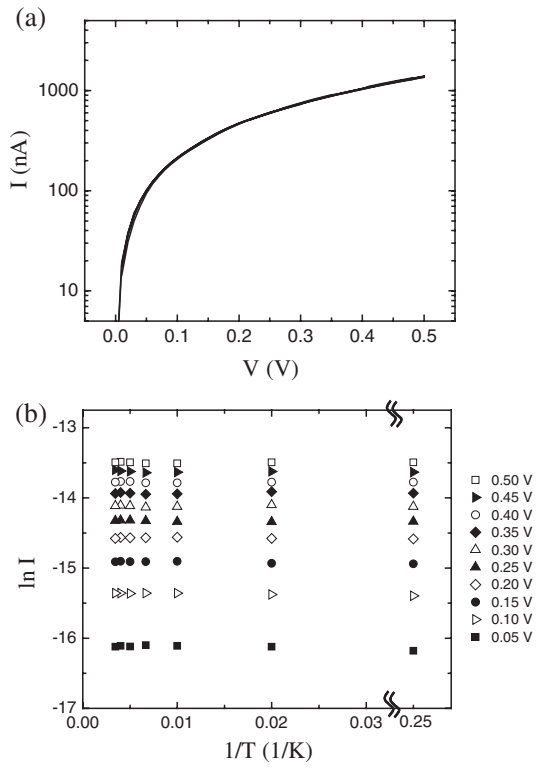

Fig. 2. (a) $I(V,T)$ characteristics of C8 dithiol SAM at selected temperatures (4.2, 50, 100, 150, 200, 250, and 290 K). (b) Arrhenius plot generated from the data in (a), at voltages from 0.05 to 0.5 V with 0.05 V steps.

which is a unitless adjustable parameter that is introduced to provide either a way of applying the tunneling model of a rectangular barrier to tunneling through a nonrectangular barrier,[4] or an adjustment to account for the effective mass (m^*) of the tunneling electrons through a rectangular barrier,[4,14,16,17] or both. $\alpha = 1$ corresponds to the case for a rectangular barrier and bare electron mass. By fitting individual $I(V)$ data using eq. (1), Φ_B and α values can be obtained. The optimum fitting results obtained with $\Phi_B = 1.20 \pm 0.06$ eV and $\alpha = 0.59 \pm 0.01$ for the C8-dithiol device are shown as solid curves in $I(V)$ plots on the linear (Fig. 3(a)) and log scale (Fig. 3(b)), where the error ranges of Φ_B and α are dominated by potential device size fluctuations. A contact junction area of 51 ± 5 nm in diameter (obtained from statistical study of the test devices with a scanning electron microscope) and molecular length of 15.1 Å (by considering an Au-thiol bonding length[18]) were used in the fittings. A current density J of $(8.8 \pm 1.8) \times 10^4$ A/cm^2 at 1.0 V is calculated. The α parameter fit presented above corresponds to an effective mass m^* ($= \alpha^2$ m) of 0.35 m.

It is interesting to compare tunneling parameters for C8-dithiol SAM with those for octanemonothiol SAM. For an octanemonothiol SAM, $\Phi_B = 1.83 \pm 0.10$ eV, $\alpha = 0.61 \pm 0.01$ (molecular length of 13.3 Å was used), $m^* = 0.37$ m, and $J = (3.1 \pm 1.0) \times 10^4$ A/cm^2 at 1.0 V (junction area of 50 ± 8 nm in diameter was used) have been reported.[19] Although the C8-dithiol is longer than octanemonothiol in the molecular length, the current density for C8-dithiol is larger. This can be explained by the difference of metal-

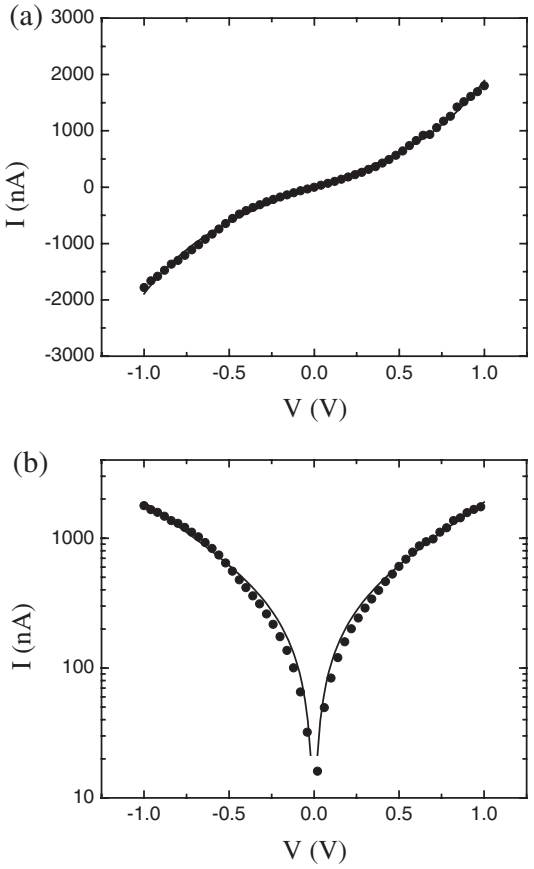

Fig. 3. Measured C8-dithiol $I(V)$ data (circular symbols) is compared with calculation (solid curve) using the optimum fitting parameters of $\Phi_B = 1.20\,\text{eV}$ and $\alpha = 0.59$. Current is plotted (a) on linear scale and (b) on log scale.

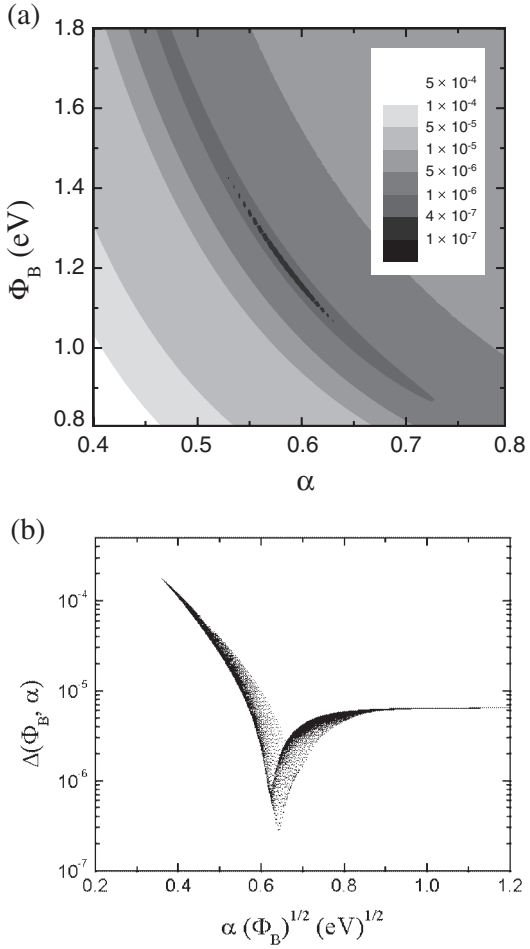

Fig. 4. (a) Contour plot of $\Delta(\Phi_B, \alpha)$ values for C8-dithiol device as a function of Φ_B and α, where the darker region corresponds to a better fitting. (b) A plot of $\Delta(\Phi_B, \alpha)$ as a function of $\alpha{\Phi_B}^{1/2}$.

molecule contacts between the two molecular systems; unlike physical contact of Au-CH_3 for octanemonothiol case, Au-S contact in C8-dithiol case provides a strongly coupled contact due to chemical reaction of Au and thiol, thus reducing contact barrier and increasing tunneling current. This argument is supported by absence of a strong S-H vibrational mode, discussed in the next section.

In order to investigate the dependence of the Simmons model fitting on Φ_B and α, a fitting minimization analysis was undertaken on the individual Φ_B and α values. $\Delta(\Phi_B, \alpha) = (\Sigma|I_{\text{exp,V}} - I_{\text{cal,V}}|^2)^{1/2}$ was calculated and plotted where $I_{\text{exp,V}}$ is the experimental current-voltage values and $I_{\text{cal,V}}$ is calculated using eq. (1). 16,000 different $\{\Phi_B, \alpha\}$ pairs were used in the fittings with Φ_B ranging from 0.8 to 1.8 eV (0.005 eV increment) and α from 0.4 to 0.8 (0.005 increment). Figure 4(a) is the contour plot of $\Delta(\Phi_B, \alpha)$ versus Φ_B and α values generated for the C8-dithiol $I(V)$ data where darker regions correspond to smaller $\Delta(\Phi_B, \alpha)$. The darker regions represent better fits of eq. (1) to the measured $I(V)$ data. Although the parameters for the smallest $\Delta(\Phi_B, \alpha)$ is consistent with those determined from the previous Simmons tunneling fitting $\{\Phi_B = 1.20\,\text{eV}$ and $\alpha = 0.59\}$, one can see there is a distribution of other Φ_B and α values yielding dark regions. A plot of $\Delta(\Phi_B, \alpha)$ versus $\alpha{\Phi_B}^{1/2}$ for the same device reveals a more pronounced dependence, and is shown in Fig. 4(b). This plot indicates the fitting to the Simmons model sharply depends on the product of $\alpha{\Phi_B}^{1/2}$.[19] For this plot the $\Delta(\Phi_B, \alpha)$ is minimized at $\alpha{\Phi_B}^{1/2}$ of 0.64 $(\text{eV})^{1/2}$. As explained shortly, this value corresponds to a zero field decay coefficient β_0 of $0.66\,\text{Å}^{-1}$.

The decay coefficient is a characteristic quantity of tunneling media. In addition to the temperature-independency of tunneling transport, another distinct property of tunneling is exponential length dependence. The tunneling current is exponentially dependent on the barrier length (molecular length in our systems) as $J \propto \exp(-\beta d)$,[4,13] where β is decay coefficient. For alkanemonothiol SAMs, bias-dependent β values have been observed with a zero field decay coefficient β_0 of $0.79\,\text{Å}^{-1}$ from measurements on different length molecules.[4] When different length molecules are not used, at least β_0 value can be calculated using Φ_B and α values obtained from individual $I(V)$ data fittings from[4,19]

$$\beta_0 = \frac{2(2m)^{1/2}}{\hbar}\alpha(\Phi_B)^{1/2} \tag{2}$$

Using $\alpha{\Phi_B}^{1/2}$ of 0.64 $(\text{eV})^{1/2}$ for minimum $\Delta(\Phi_B, \alpha)$ in Fig. 4(b), a β_0 of $0.66\,\text{Å}^{-1}$ can be calculated from eq. (2). This calculated β_0 value for octanedithiol is smaller than the value $0.79\,\text{Å}^{-1}$ for alkanemonothiol[4] and other β values reported by other groups for alkanemonothiols.[20] For

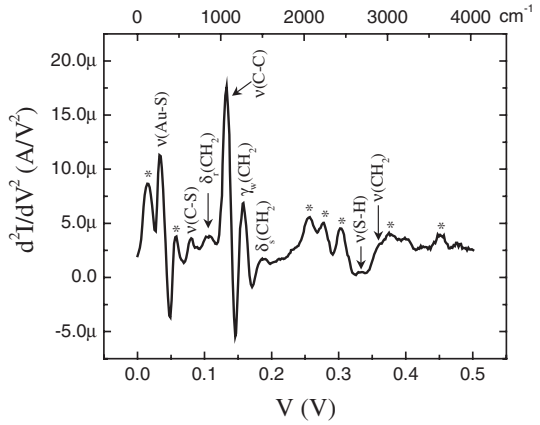

Fig. 5. Inelastic electron tunneling spectra of C8-dithiol SAM obtained from lock-in second harmonic measurements with an AC modulation of 8.70 mV (RMS value) at a frequency of 503 Hz ($T = 4.2$ K). Peaks labeled* are most probably background due to the encasing Si_3N_4.

alkanedithiols, Xu, *et al.*, reported a β value of $0.80 \pm 0.08\,\text{Å}^{-1}$ (converted from 1.0 ± 0.1 per methylene) by scanning tunneling microscopy[21] and Cui, *et al.*, reported $0.46 \pm 0.02\,\text{Å}^{-1}$ (converted from 0.57 ± 0.03 per methylene) by using a conducting atomic force microscope technique.[22] However SPM techniques can have systematic errors that requires careful analysis[19] and cannot be checked against variable temperature studies. Our value of $0.66\,\text{Å}^{-1}$ is from variable temperature measurements. Further detailed length dependent studies should provide a more accurate value.

Table I. Summary* of the major vibrational modes of alkanethiolates. Taken from ref. 24–26.

Modes	Methods	Wavenumber (cm^{-1})	(meV)
ν(Au-S)	HREELS	225	28
ν(C-S)	Raman	641	79
	Raman	706	88
$\delta_r(CH_2)$	HREELS	715	89
	IR	720	89
	IR	766	95
	IR	925	115
ν(C-C)	HREELS	1050	130
	Raman	1064	132
	Raman	1120	139
$\gamma_{w,t}(CH_2)$	IR	1230	152
	HREELS	1265	157
	IR	1283	159
	IR	1330	165
$\delta_s(CH_2)$	HREELS	1455	180
ν(S-H)	Raman	2575	319
$\nu_s(CH_2)$	Raman	2854	354
	HREELS	2860	355
$\nu_{as}(CH_2)$	Raman	2880	357
	Raman	2907	360
	HREELS	2925	363

*There is a vast amount of literature with spectroscopic assignments for alkanethiols. The references given are representative for IR,[24] Raman,[25] and HREELS[26] assignments.

3.2 Inelastic electron tunneling spectroscopy

Electronic transport through C8-dithiol SAM was further investigated with the technique of inelastic electron tunneling spectroscopy (IETS) to study molecular vibrational signatures.[23] Figure 5 shows the IETS spectrum of the C8-dithiol SAM device (same device used for $I(V,T)$ study) obtained at $T = 4.2$ K. An AC modulation of 8.70 mV (RMS value) at a frequency of 503 Hz was applied to the sample to acquire the second harmonic signals. The spectra are stable and repeatable upon successive bias sweeps. The spectrum at 4.2 K is characterized by three pronounced peaks at 33, 133, and 158 mV. From comparison with previously reported infrared (IR), Raman, and high resolution electron energy loss (HREEL) spectra of SAM covered gold surfaces (Table I), these three peaks are assigned to ν(Au-S), ν(C-C), and $\gamma_w(CH_2)$ modes of a surface bound alkanethiolate.[24–27] The absence of a strong ν(S-H) signal at $\sim$329 mV suggests that most of the thiol groups have reacted with both the gold bottom and top contacts. Peaks are also reproducibly observed at 80, 107, and 186 mV. They correspond to ν(C-S), $\delta_r(CH_2)$, and $\delta_s(CH_2)$ modes. The stretching mode of the CH_2 groups, $\nu(CH_2)$, appears as a shoulder at 357 meV. The peak at 15 mV is due to vibrations from either Si, Au, or δ(C-C-C).[28–30] We note that all alkanethiolate peaks without exception or omission occur in the spectra. Peaks at 58, 257, 277, and 302, as well as above 375 mV are likely to originate from Si-H and N-H vibrations related to the silicon nitride membrane,[28,31,32] which forms the SAM encasement. Measurement of the background spectrum of an "empty" nanopore device with only gold contacts to obtain background contributions from Si_3N_4 is hampered by either too low (open circuit) or too high (short circuit) currents in such a device. However, to the best of our knowledge alkanethiols have no vibrational signatures in these regions. Similar IETS result has also been obtained using a different test structure recently.[33]

Although there are no selection rules in IETS as there are in IR and Raman spectroscopy, certain selection preferences have been established. According to the IETS theory,[34] molecular vibrations with net dipole moments perpendicular to the interface of the tunneling junction have larger peak intensities than vibrations with net dipole moments parallel to the interface (for dipoles close to the electrodes). Thus vibrations perpendicular to the electrode interface, i.e., ν(Au-S), ν(C-S), ν(C-C), and $\gamma_w(CH_2)$ dominate the IETS spectrum while modes parallel to the interface, i.e., $\delta_{r,s}(CH_2)$ and $\nu(CH_2)$, are weak, as clearly shown in Fig. 5. Note that the signals of Fig. 5 are the average effect of many molecules because there are thousands of molecules in the junction. By comparing the intensity of each vibrational mode according to the intensity preference rules, Fig. 5 indicates the majority of molecules are standing (either tilted or not) as schematically illustrated in Fig. 1(a).

In order to verify that the observed spectra are indeed valid IETS data, the peak width broadening was examined as a function of temperature and modulation voltage. IETS was performed with different AC modulations at a fixed temperature, and at different temperatures with a fixed AC

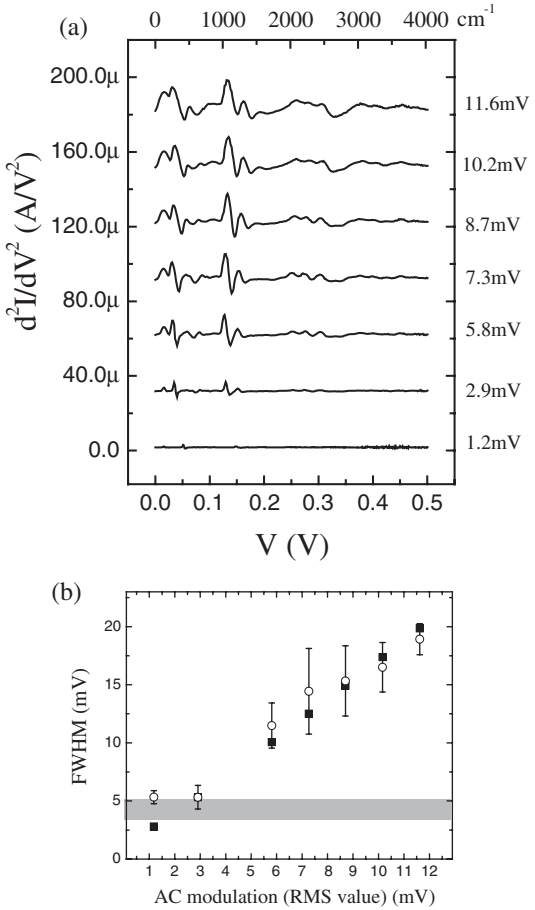

Fig. 6. (a) Modulation dependence of IETS spectra obtained at 4.2 K. (b) Line (C-C stretching mode) broadening as a function of AC modulation. The circular symbols are experimental FWHMs and the square symbols are theoretical calculations considering both modulation and thermal contributions. The shaded bar denotes the expected saturation due to the derived intrinsic linewidth (including a 5.4 k_BT thermal contribution) of 3.73 ± 0.98 meV.

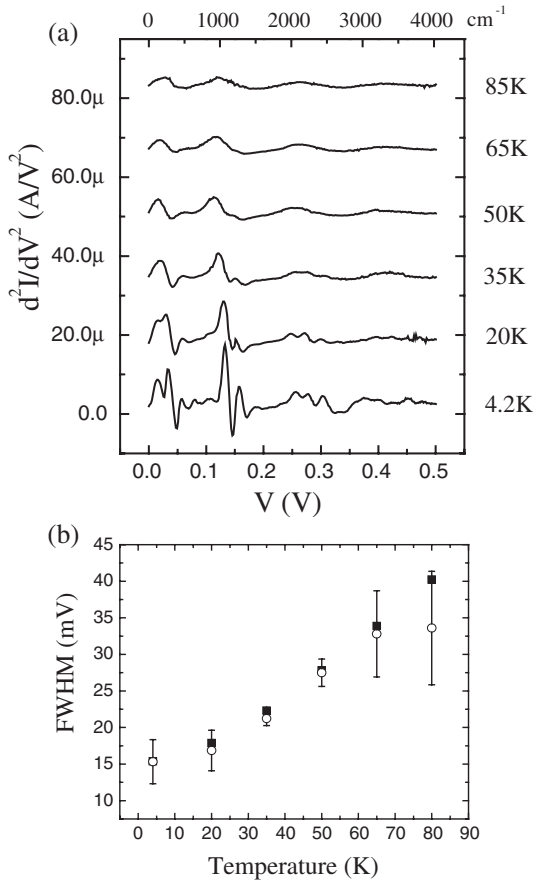

Fig. 7. (a) Temperature dependence of IETS spectra. (b) Line (C-C stretching mode) broadening as a function of temperature at a fixed AC modulation (8.70 mV). The circular symbols are experimental FWHMs and the square symbols are theoretical calculations considering thermal broadening, modulation broadening, and the intrinsic linewidth.

modulation. Figure 6(a) shows the modulation dependence of the IETS spectra obtained at 4.2 K, and Fig. 6(b) shows the modulation broadening of the C-C stretching mode at 133 meV. The circular symbols are the full widths at half maximum (FWHMs) of the experimental peak at $T = 4.2$ K at various modulation voltages. A Gaussian distribution function was utilized to obtain a FWHM and the error range.[35] The square symbols are calculated FWHM values ($W_{\text{theoretical}}$) taking into account both a finite temperature effect and a finite voltage modulation effect. The thermal broadening effect ($W_{\text{thermal}} \sim 5.4\,\text{kT}$) is due to the smearing in the energy of the electron distribution in the metal electrodes,[11] and the voltage modulation broadening effect ($W_{\text{modulation}} \sim 1.7\,V_{\text{ac\_rms}}$) is an instrumental effect because one can only apply a finite modulation of the voltage to obtain second harmonic signal.[36] These two broadening contributions add as the squares: $W^2{}_{\text{theoretical}} = W^2{}_{\text{thermal}} + W^2{}_{\text{modulation}}$. The agreement is excellent over most of the modulation range, but we note a saturation of the linewidth at low modulation voltage indicating the influence of a non-negligible intrinsic linewidth. Taking into account the known thermal and modulation broadenings, and including the intrinsic linewidth (W_I)[37] broadening as a fitting parameter, the measured peak width (W_{exp}) is given by

$$W_{\text{exp}} = \sqrt{W_I^2 + W_{\text{thermal}}^2 + W_{\text{modulation}}^2} \tag{3}$$

W_I can be determined by using a nonlinear least squares fit to the AC modulation data (Fig. 6(b)) with eq. (3), giving an intrinsic linewidth of 3.73 ± 0.98 meV for this C-C stretching mode. This is shown (with the error range) in Fig. 6(b) as a shaded bar including the thermal contribution.

We can independently check the thermal broadening at fixed modulation width. Figure 7(a) shows the temperature dependence of the IETS spectra obtained with an AC modulation of 8.70 mV. In Fig. 7(b) the circular symbols (and corresponding error bars) are experimental FWHM values of the C-C stretching mode from Fig. 7(a), determined by a Gaussian fit (and error of the fit) to the experimental lineshape. For simplicity we have only considered Gaussian lineshapes[35] resulting in increased error bars for the lower temperature range due to an asymmetric lineshape. The square symbols are theoretical calculations considering thermal broadening, modulation broadening, and the intrinsic linewidth determined above. The error ranges of the calculation (due to the intrinsic linewidth error) are approximately the size of the data points. The agreement between theory and experiment is

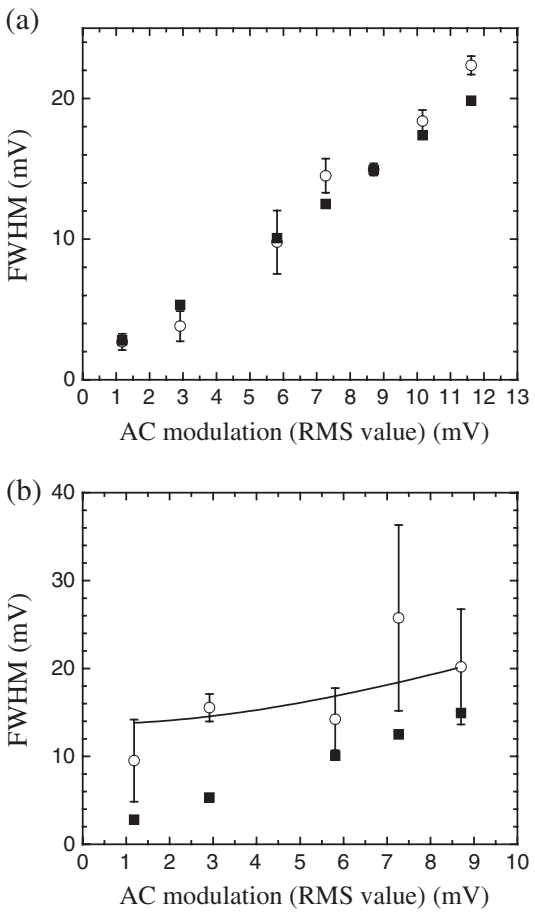

Fig. 8. Line broadenings as function of AC modulation for IETS spectra obtained at 4.2 K for (a) the Au-S stretching mode and (b) the CH_2 wagging mode. The circular symbols are experimental FWHMs and the square symbols are theoretical calculations considering modulation and thermal contributions. Nonlinear least squares fitting to eq. (3) to determine intrinsic linewidth is shown as the solid curve in (b).

very good, spanning a temperature range from below ($\times 0.5$) to above ($\times 10$) the thermally broadened intrinsic linewidth. This linewidth should be a sensitive test to compare to theoretical models of transmission probabilities.[38)]

Similar intrinsic linewidths have been determined for the Au-S stretching mode (33 meV) and CH_2 wagging mode (158 meV), and the results are shown in Fig. 8. For the Au-S stretching mode, the deviation of experimental data from calculated values is little (Fig. 8(a)), indicating that its intrinsic linewidth is small. A linewidth upper limit of 1.69 meV is determined for this vibrational mode. For CH_2 wagging mode, nonlinear least squares fit to eq. (3) (solid curve in Fig. 8(b)) gave intrinsic linewidth of 13.5 ± 2.4 meV. The linewidths and their variation throughout the molecule are potentially due to inhomogeneous configuration of the molecular constituents, and a more detailed understanding may give detailed structural information of these device structures.

4. Conclusions

In conclusion, the electronic transport through self-assembled C8-dithiol monolayers was investigated. Tunneling transport was observed as the main conduction mechanism by temperature-independent $I(V)$ characteristics. IETS study of a C8-dithiol SAM device exhibited that tunneling charge carriers couple with molecular vibrations, clearly indicating molecular presence and thus intrinsic molecular transport. Observed IETS peak intensities and widths of the inelastic tunneling spectra agree well with theoretical predictions.

Acknowledgements

The authors would like to thank J. F. Klemic, X. Li, and R. Munden for helpful discussions and assistance. We especially thank I. Kretzschmar for assistance in identification of the IETS spectra. This work was supported by DARPA/ONR (N00014-01-1-0657), ARO (DAAD19-01-1-0592), AFOSR (F49620-01-1-0358), NSF (DMR-0095215), and NASA (NCC 2-1363). T. Lee thank Brain Korea 21 Project for his financial support.

1) *Molecular Nanoelectronics*, eds. M. A. Reed and T. Lee (American Scientific Publishers, Stevenson Ranch, 2003).
2) A. Nitzan and M. A. Ratner: Science **300** (2003) 1384.
3) A. Ulman: *An Introduction to Ultrathin Organic Films from Langmuir-Blodgett to Self-Assembly* (Academic Press, Boston, 1991).
4) W. Wang, T. Lee and M. A. Reed: Phys. Rev. B **68** (2003) 035416.
5) M. A. Ratner, B. Davis, M. Kemp, V. Mujica, A. Roitberg and S. Yaliraki: *Molecular Electronics: Science and Technology*, eds. A. Aviram and M. A. Ratner (The Annals of the New York Academy of Sciences, New York, 1998) Vol. 852.
6) R. C. Jaklevic and J. Lambe: Phys. Rev. Lett. **17** (1966) 1139.
7) C. J. Adkins and W. A. Phillips: J. Phys. C: Solid State Phys. **18** (1985) 1313.
8) *Tunneling Spectroscopy: Capabilities, Applications, and New Techniques*, ed. P. K. Hansma (Plenum, New York, 1982).
9) B. C. Stipe, M. A. Rezaei and W. Ho: Science **280** (1998) 1732.
10) C. Zhou, M. R. Deshpande, M. A. Reed, L. Jones II and J. M. Tour: Appl. Phys. Lett. **71** (1997) 611.
11) J. Lambe and R. C. Jaklevic: Phys. Rev. **165** (2968) 821.
12) P. Horowitz and W. Hill: *The Art of Electronics* (Cambridge University Press, New York, 1989).
13) S. M. Sze: *Physics of Semiconductor Devices* (Wiley, New York, 1981).
14) R. Holmlin, R. Haag, M. L. Chabinyc, R. F. Ismagilov, A. E. Cohen, A. Terfort, M. A. Rampi and G. M. Whitesides: J. Am. Chem. Soc. **123** (2001) 5075.
15) J. G. Simmons: J. Appl. Phys. **34** (1963) 1793.
16) C. Joachim and M. Magoga: Chem. Phys. **281** (2002) 347.
17) J. K. Tomfohr and O. F. Sankey: Phys. Rev. B **65** (2002) 245105.
18) D. J. Wold, R. Haag, M. A. Rampi and C. D. Frisbie: J. Phys. Chem. B **106** (2002) 2813.
19) T. Lee, W. Wang, J. F. Klemic, J. Zhang, J. Su and M. A. Reed: J. Phys. Chem. B **108** (2004) 8742.
20) See ref. 19 for summary of reported β values for alkanemonothiols.
21) B. Xu and N. J. Tao: Science **301** (2003) 1221.
22) X. D. Cui, A. Primak, X. Zarate, J. Tomfohr, O. F. Sankey, A. L. Moore, T. A. Moore, D. Gust, L. A. Nagahara and S. M. Lindsay: J. Phys. Chem. B **106** (2002) 8609.
23) W. Wang, T. Lee, I. Kretzschmar and M. A. Reed: Nano Lett. **4** (2004) 643.
24) C. Castiglioni, M. Gussoni and G. Zerbi: J. Chem. Phys. **95** (2992) 7144.
25) M. A. Bryant and J. E. Pemberton: J. Am. Chem. Soc. **113** (1991) 8284.
26) H. Kato, J. Noh, M. Hara and M. Kawai: J. Phys. Chem. B **106** (2003) 9655.
27) The symbols δ, γ, and ν denote in-plane rocking (r) and scissoring (s), out-of-plane wagging (w) and twisting (t), and stretching modes, respectively.
28) M. Molinary, H. Rinnert, M. Vergnat and P. Weisbecker: Mater. Sci. & Eng. B **69** (2003) 301.

29) P. D. Bogdanoff, B. Fultz and S. Rosenkranz: Phys. Rev. B **60** (1999) 3976.
30) U. Mazur and K. W. Hipps: J. Phys. Chem. **86** (2983) 2854.
31) U. Mazur and K. W. Hipps: J. Phys. Chem. **85** (1981) 2244.
32) H. Kurata, M. Hirose and Y. Osaka: Jpn. J. Appl. Phys. **20** (1981) L811.
33) J. G. Kushmerick, J. Lazorcik, C. H. Patterson, R. Shashidhar, D. S. Seferos and G. C. Bazan: Nano Lett. **4** (2004) 639.
34) J. Kirtley and J. T. Hall: Phys. Rev. B **22** (1980) 848.
35) I. J. Lauhon and W. Ho: Phys. Rev. B **60** (1999) R8525.
36) J. Klein, A. Léger, M. Belin, D. Défourneau and M. J. L. Sangster: Phys. Rev. B **7** (1973) 2336.
37) I. J. Lauhon and W. Ho: Rev. Sci. Instrum. **72** (2001) 216.
38) M. A. Kastner: Phys. Today **January** (1993) 24.